Hindawi
Journal of Nanomaterials
Volume 2019, Article ID 2394184, 8 pages
https://doi.org/10.1155/2019/2394184

Research Article

Preparation and Adsorption Properties of Biochar/g-C_3N_4 Composites for Methylene Blue in Aqueous Solution

Xiaodong Li

Department of Basic Science, Jilin Jianzhu University, Changchun 130118, China

Correspondence should be addressed to Xiaodong Li; lxdjlju@163.com

Received 11 January 2019; Accepted 17 March 2019; Published 10 June 2019

Academic Editor: Giuseppe Compagnini

Using straw and urea as raw materials, biochar (BC) and g-C_3N_4 were prepared by oxygen-free pyrolysis at 300°C and 550°C. BC/g-C_3N_4 was prepared by loading different amounts of g-C_3N_4 onto the surface of biochar and characterized by SEM and FT-IR. The adsorption effect on methylene blue (MB) was investigated from the aspects of dosage and pH. The studies of adsorption equilibrium isotherms and the kinetic and the thermodynamic parameters on the BC/g-C_3N_4 adsorbents are discussed. The results showed that BC/g-C_3N_4 0.16 g/L with a doping ratio of 1 : 3 was added to the MB solution with an initial concentration of 50 mg/L and pH = 11. The adsorption rate and adsorption amount were 96.72% and 302.25 mg/g, respectively. The adsorption process included surface adsorption and intraparticle diffusion, which conformed to the pseudo-second-order kinetic model and Langmuir-Freundlich model. Thermodynamic parameters ($\Delta G^0 < 0$, $\Delta H^0 > 0$, and $\Delta S^0 > 0$) showed that the adsorption reaction is spontaneous, which positively correlated with temperature.

1. Introduction

Agriculture, forestry, and food processing produce large amounts of biomass waste every year, among which straw accounts for the largest share of agricultural waste, with an annual output of about 731 million tons [1]. Its main components include cellulose (35-40 wt%), hemicellulose (20-25 wt%), lignin (20-27 wt%), and ash (10-15 wt%) [2]; it is a kind of low-quality dietary fiber plant, used as feed, which can cause indigestion in animals and has limited biodegradability [3]. Turning biowaste into high value-added carbon materials such as biofuels and derived materials is a more environmentally friendly way of recycling. Compared with activated carbon, biochar produced by oxygen limitation pyrolysis of biological waste has a strong adsorption capacity [4]; its production cost is lower, and it has a good adsorption effect on various dyes [5, 6]. Methylene blue (MB) is a conjugated heterocyclic cationic dye with thiazine structure. It accumulates in large amounts in the ecological environment, which will seriously affect photosynthesis in the aquatic environment and may cause cancer and mutagenesis [7]. At present, treatment methods mainly include oxidation method [8], biological method [9], and adsorption method, among which adsorption method is a fast, inexpensive, and universal treatment method [10].

The combination of biochar with inorganic and magnetic nanomaterials can greatly improve its structure and performance. Graphitic carbon nitride (g-C_3N_4) not only has a high specific surface area but also the chemical functional groups on the surface can provide highly compatible active sites, thus increasing the complex ability of nanomaterials to pollutants. In this experiment, biochar and g-C_3N_4 were prepared by pyrolysis, and biochar carbonitride carbon (BC/g-C_3N_4) was synthesized by impregnation method. The purpose of the study was to evaluate the adsorption capacity of BC/g-C_3N_4 while removing the MB in wastewater. In addition, a suitable kinetic and equilibrium isotherm model was identified in order to describe the current adsorption process employed using BC/g-C_3N_4.

2. Experimental

2.1. Preparation of BC/g-C_3N_4. Preparation of BC: the washed and dried straw was cut into segments of about 2 cm in

length, placed in a covered ceramic crucible, heated to a temperature of 15°C/min to 300°C for 5 h, and taken out after natural cooling to room temperature. After passing through the 150-mesh standard sieve, BC was obtained.

Preparation of g-C_3N_4: took a certain amount of urea, placed in a ceramic crucible with a cover, rising at a rate of about 5°C/min to 550°C heat for 4 h, taken out after cooling to room temperature, and after passing through the 150-mesh standard sieve, g-C_3N_4 was obtained.

Preparation of BC/g-C_3N_4: took a certain amount of BC and g-C_3N_4 and placed in a beaker, deionized water was added and ultrasonic suspension was formed, and mixed according to certain proportion immersion, ultrasonic 30 min, 40°C stir 2 h, 60°C drying to constant weight.

2.2. Batch Adsorption Experiment. The pollutant concentration was initially measured. At different temperatures, a certain concentration of MB solution was taken in a 250 mL conical flask. The pH value was adjusted, and a certain amount of samples with different doping ratios was added. All the experiments were performed using a batch process. A UV-visible spectrophotometer (UV-1700) was used to measure the residual solution after filtering the suspensions. Equations (1) and (2) were used to calculate the adsorption capacity of the pollutants. The adsorption behaviors of BC/g-C_3N_4 were determined by examining the rate of removal of MB dissolved in an aqueous solution.

$$q_t = \frac{(C_0 - C_t)V}{m}, \quad (1)$$

$$\eta = \frac{1 - C_t}{C_0}, \quad (2)$$

where C_0 and C_t (mg/L) are the initial and final equilibrium concentrations of MB in a solution, respectively, V (mL) is the volume of the solution, and m (mg) is the mass of the adsorbent.

2.3. Characterization and Analysis. The morphology of BC/g-C_3N_4 was characterized by scanning electron microscope (SEM) (JSM-5600LV, JEOL, Japan). Surface functional group characteristics of BC/g-C_3N_4 were determined by FT-IR Spectrum-100 Fourier-transform infrared spectrometer using conventional KBr pellets in the 4000-400 cm^{-1} range.

3. Results and Discussion

3.1. Characterization Analysis. The microscopic morphology of BC was a massive and zonal porous structure (Figure 1(a)). Figure 1(b) shows the local diagram of the composite material. g-C_3N_4 bound to the sites on the surface of BC, and the coverage was relatively uniform and dispersed.

A large number of functional groups existed on the surface of the sample, which played an important role in the adsorption process (Figure 2) [11]. Three groups of samples had characteristic peaks at 3400-3440 cm^{-1}, indicating the stretching vibration of hydroxyl or amino, and the bending vibration peaks of C-H aromatic ring at 790-810 cm^{-1}. In sample BC, at 1620 cm^{-1}, the tensile vibration of C=O bond in -COOH- and -$CONH_2$ appeared. At 1100 cm^{-1} was the stretching vibration of C-O in cellulose, hemicellulose, and lignin or C-O-C in cellulose and hemicellulose. Sample g-C_3N_4 has a C≡N peak at 2180 cm^{-1}. At 1610, 1250, and 1400 cm^{-1}, there existed a series of stretching vibration peaks of C=N, C-N, and extracyclic C-N on a carbon-nitrogen heterocycle. The peak shape of BC/g-C_3N_4 was basically consistent with that of g-C_3N_4, and the characteristic peak was weakened, which indicated that g-C_3N_4 and BC were not simply physically mixed but formed a compact structure with lower energy.

3.2. Effect of Components and Doping Ratio. The adsorption performance of BC, g-C_3N_4, and BC/g-C_3N_4 composites with various doping ratios on MB at room temperature is shown in Figure 3. As seen from Figure 3(a), the adsorption basically reached equilibrium after 60 min and the adsorption capacity of the composite was 2.70 times and 3.76 times higher than that of the single component, respectively. g-C_3N_4 was loaded on the surface of BC, which increased its surface area and surface functional groups and significantly improved its adsorption performance. When the content of g-C_3N_4 was too low, it could not be completely coated on the surface of BC, only individual sites exist and were unevenly dispersed. When g-C_3N_4 continued to increase, the excess part agglomerates on the surface of the BC, which reduced the attachment point of MB on the composite and also weakened the force between the functional groups. The effect of the doping ratio of BC : g-C_3N_4 was also investigated (Figure 3(b)). The results indicated that by increasing the amount of g-C_3N_4, the adsorption amount of 145 mg/g to 190 mg/g, the adsorption efficiency of BC/g-C_3N_4 increases from 69.92% to 95.32%. However, when the doping ratio of BC : g-C_3N_4 exceeded 1 : 3, the adsorption amount of BC/g-C_3N_4 decreased with increasing the amount of g-C_3N_4. Obviously, the removal efficiency of MB onto BC/g-C_3N_4 by biosorption is rapid initially and then slows down gradually until it comes to a state of equilibrium; this is probably due to initially a large number of vacant surface sites which are available for biosorption, while progressively fewer remaining sites become increasingly difficult to occupy due to the existence of the repulsive forces between the solute molecules of the solid and bulk phases.

3.3. Effect of pH on Adsorption. The variation in the adsorption of the dyes was studied in the pH range of 1-10, and the results are shown in Figure 4. The adsorption amount at pH = 11 was about 6 times higher than that at pH = 2, indicating that the alkaline environment was more favorable for the adsorption of MB on the composite. When the pH of the solution is low, a large amount of H^+/H_3O^+ existed in the solution, occupying the binding sites provided by functional groups such as -OH and -COOH. The surface of the biochar was protonated, and increased positive charge generates impulse effect [12]. The MB is cationic. Therefore, the higher uptake of MB on BC/g-C_3N_4 at high pH may result due to the neutralization of the negative charge at the surface of the adsorbent. With the increase of pH, the concentration of H^+/H_3O^+ ions in the solution decreased

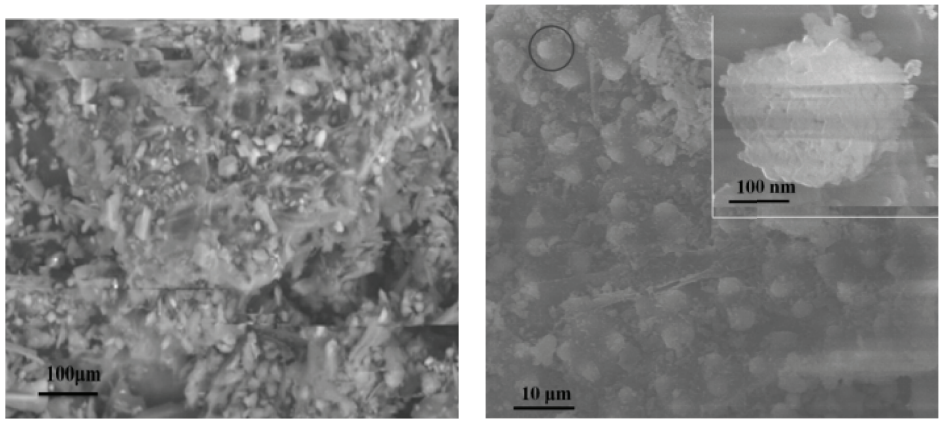

(a) (b)

Figure 1: (a) BC of SEM. (b) BC/g-C_3N_4 of SEM.

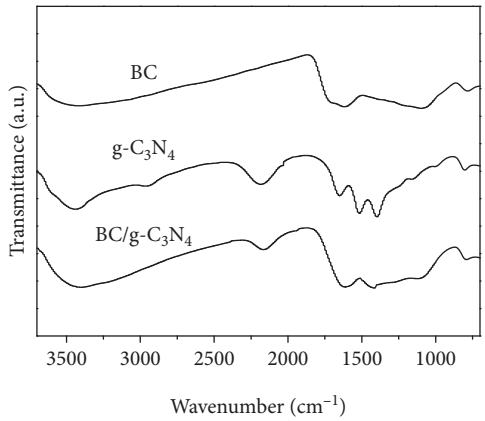

Figure 2: The FT-IR spectra of BC, g-C_3N_4, and BC/g-C_3N_4.

and the electrostatic attraction between MB and the adsorbent increased. Meanwhile, the concentration difference between H^+ and OH^- in the solution gradually decreased and the protonation/deprotonation effect on the surface of the adsorbent was not obvious, so the adsorption amount of MB increased and the adsorption isotherms gradually flattened [13]. On the contrary, a slight fall in the amount of dye adsorbed with decreasing pH may be due to the repulsion between species with the same charge.

3.4. Effect of Dosage on Adsorption. The pH of aqueous solutions is 11; the effect of BC/g-C_3N_4 dose on the MB removal is presented in Figure 5. As seen in Figure 5, due to the limited amount of MB in the solution, the adsorption amount of BC/g-C_3N_4 decreased with the increase of dosage and the excessive adsorption of adsorbent will lead to excess adsorption point. When increasing from 0.04 g/L to 0.32 g/L, the adsorption amount of biochar to MB decreased from 918.9 mg/g to 153.45 mg/g. When the dosage was 0.04~0.08 g/L, the composite material could provide more sufficient adsorption combination point for MB so that the removal rate of MB increased rapidly. When the dosage exceeds 0.08 g/L, the adsorption rate of MB was more than 90%. When the dosage was 0.32 g/L, the adsorption rate was as high as 98.21% and was almost complete adsorption. Considering the adsorption amount, removal rate, and cost, 0.16 g/L was used as optimal amount for further experiments.

3.5. Adsorption Kinetics. In order to study the adsorption mechanism, chemical reaction, diffusion control, mass transfer, and other potential rate control steps, in this paper, the pseudo-first-order kinetic, pseudo-second-order kinetic, Elovich, and intraparticle diffusion models were adopted to perform nonlinear fitting of experimental data [14]. The fitting results are shown in Figure 6 and Table 2.

$$\begin{aligned}
\text{The pseudo-first-order kinetic model } Q_t &= Q_e\left(1 - e^{-K_1 t}\right),\\
\text{The pseudo-second-order kinetic model } Q_t &= \frac{Q_e^2 K_2 t}{1 + Q_e K_2 t},\\
\text{Elovich equation } Q_t &= A + B \ln t,\\
\text{The intraparticle diffusion model } Q_t &= K_i t^{1/2} + C_i,
\end{aligned} \tag{3}$$

where Q_e is the equilibrium adsorption capacity of MB; t is the adsorption time; K_1, K_2, and K_i are the rate constants of each model; A, B, and C_i are the correlation constants, respectively; and i is the intraparticle diffusion stage.

Figure 6(a) shows the adsorption kinetics of MB solution on BC/g-C_3N_4, and the relevant fitting parameters are given in Table 2. The equilibrium was quickly reached. Kinetic adsorption data were analyzed using the pseudo-first-order kinetic model, the pseudo-second-order kinetic model, Elovich equation, and the intraparticle diffusion model. The determination of the different rate constants shows that the model of pseudo second order with a good correlation coefficient ($R^2 = 0.966$) is the most reliable. Meanwhile, the pseudo-second-order kinetic equation could better describe the whole process of BC/g-C_3N_4 adsorption MB. The pseudo-first-order kinetic is usually applied to pure physical adsorption, where the adsorption rate is proportional to the solute concentration. The pseudo-second-order kinetic is based on the assumption that the rate-limiting step

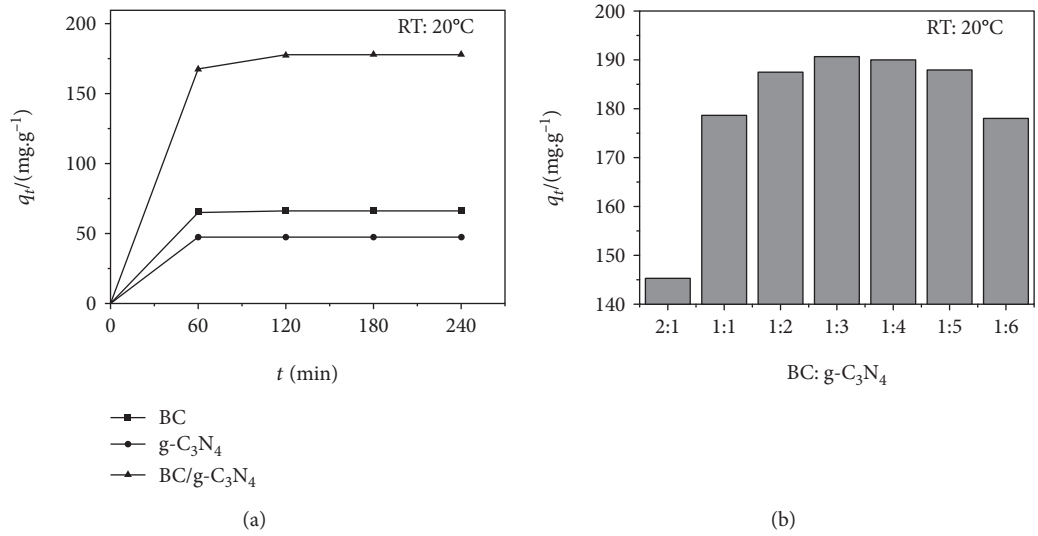

Figure 3: (a) Effect of components on adsorption. (b) Effect of doping ratio on adsorption.

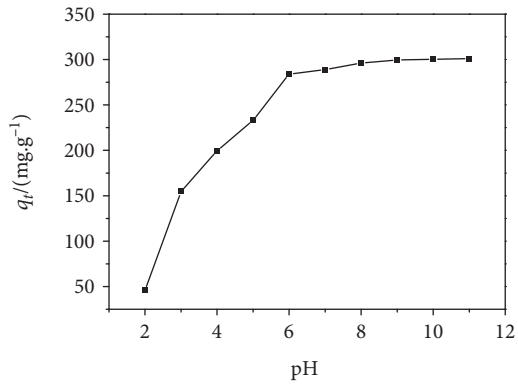

Figure 4: Effect of pH on adsorption.

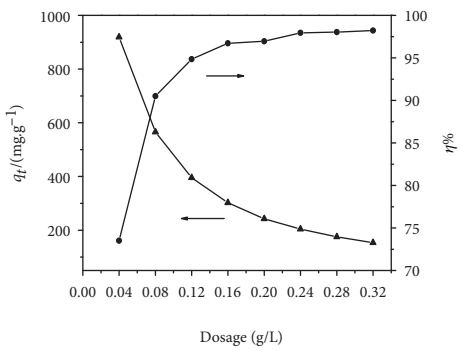

Figure 5: Effect of dosage on adsorption.

is chemisorption or physicochemical adsorption. The adsorption process includes electron transfer and exchange, forming bond. Therefore, it could be preliminarily judged that the adsorption of BC/g-C_3N_4 on dyes contained a chemical action [15]. The Elovich model describes a nonuniform diffusion process that is coordinated by reaction rates and diffusion factors. The correlation coefficient value was high $R^2 = 0.902$, indicating that the adsorption of MB on BC/g-C_3N_4 was a heterogeneous diffusion process rather than a simple first-order reaction. The results are consistent with the pseudo-second-order kinetic model.

In order to determine the control steps of MB adsorption on BC/g-C_3N_4, the experimental data were fitted using the intraparticle diffusion model. The fitting results are shown in Figure 6(b) and Table 3. The fitted line was divided into two phases. In the first stage, MB diffused from the solution to the surface of BC/g-C_3N_4. In the second stage, MB diffused into the interior of BC/g-C_3N_4. Both stages of the fitted lines did not pass the zero point, indicating that intraparticle diffusion was not the only rate control step [16]. The adsorption rate may also be affected by out-diffusion (surface adsorption and liquid film diffusion). From Table 3, it could be seen that K_1 was significantly greater than K_2, indicating that the initial stage had a rapid adsorption rate and the fitting lines of stage 2 were almost horizontal. The adsorption was the rate-controlling step in stage 2. With the adsorption, the concentration of MB in the solution decreased and K_2 decreased significantly, finally reaching the equilibrium state of adsorption.

3.6. Isothermal Adsorption and Thermodynamics. In order to describe the adsorption isotherm process of MB on BC/g-C_3N_4, the experimental data were nonlinearly fitted by Langmuir-Freundlich, Langmuir, Freundlich, and Temkin models.

$$\text{Langmuir-Freundlich model } Q_e = \frac{Q_m K_L c_e^a}{1 + K_L c_e^a}, \tag{4}$$

$$\text{Langmuir model } Q_e = \frac{Q_m K_L c_e}{1 + K_L c_e}, \tag{5}$$

$$\text{Freundlich model } Q_e = K_F c_e^{1/n}, \tag{6}$$

$$\text{Temkin model } Q_e = D + E \ln c, \tag{7}$$

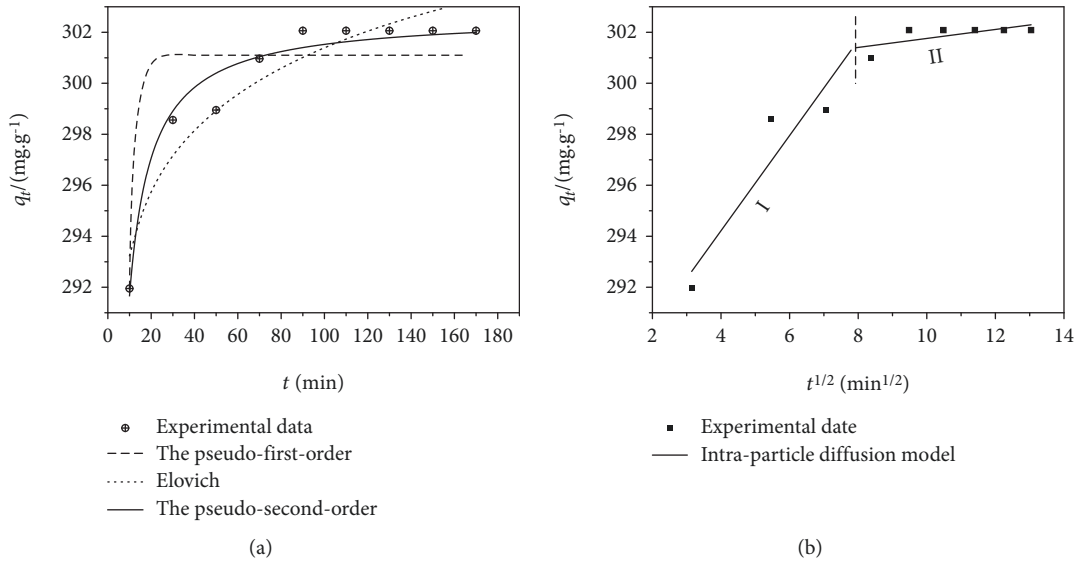

Figure 6: (a) Adsorption kinetics of BC/g-C_3N_4 on MB. (b) Intraparticle diffusion plots for the MB adsorption onto BC/g-C_3N_4.

Table 1: The main pore properties of BC/g-C_3N_4.

Sample	Specific surface area ($m^2 \cdot g^{-1}$)	Porous volume ($cm^3 \cdot g^{-1}$)	Pore size (nm)
BC/g-C_3N_4	44.36	0.04	3.68

where Q_m is the theoretical maximum adsorption amount, K_L is the Langmuir model constant, c_e is the MB mass concentration at the adsorption equilibrium, α is the Langmuir-Freundlich model constant, n is the empirical constant related to the adsorption strength, K_F is the Freundlich model constant, and D and E are the Temkin model constants.

At different temperatures, the adsorption equilibrium curve of BC/g-C_3N_4 on MB (Figures 7(a)–7(c)) had a similar trend. As the concentration of MB increased, the adsorption amount also increased. When the MB concentration was greater than 200 mg/L, the adsorption was still on the rise.

Comparing the fitting parameters of the isothermal adsorption model (Table 4), it could be found that the Langmuir-Freundlich model ($R^2 > 0.99$) and the Langmuir model ($R^2 > 0.98$) well described the adsorption process. The adsorption of MB on BC/g-C_3N_4 mainly occurred on monomolecular adsorption. As the temperature increased, the maximum adsorption capacity also increased, indicating that increasing the temperature enhanced the adsorption performance. The Temkin isotherm model assumed that the heat of adsorption of all molecules in the layer decreased linearly with the coverage rather than logarithmically. The chemical adsorption process was mainly described as electrostatic action. In this study, the Temkin isotherm model R^2 was between 0.927 and 0.893, indicating that electrostatic interaction was an important mechanism affecting the interaction between BC/g-C_3N_4 and MB.

The thermodynamic parameters were calculated by the Langmuir model ($R^2 = 0.991$-0.983). The change of Gibbs free energy in the adsorption process was related to temperature T and the standard thermodynamic equilibrium constant K_0. Under infinite dilution conditions, the concentration could be used to replace the activity according to the laws of thermodynamics. The equilibrium constant (K_d) of different initial concentrations of MB can be extrapolated to zero and the equilibrium constant was obtained, and then, the dimensionless equation could be obtained [17].

$$K_d = \frac{C_{a,e}}{C_e}, \tag{8}$$

$$\mathrm{Q}_e = (C_i - C_e)\left(\frac{V}{M}\right) = C_{a,e}. \tag{9}$$

Obtained by (4), (8), and (9),

$$\frac{C_{a,e}}{C_e} = \frac{Q_m K_L}{1 + K_L C_e}\frac{M}{V} = K_d. \tag{10}$$

Under infinite dilution conditions,

$$\begin{aligned} K_0 &= \lim_{C_e \to 0} K_d = \lim_{C_e \to 0}\left(\frac{Q_m K_L}{1 + K_L C_e}\frac{M}{V}\right) = Q_m K_L \frac{M}{V}, \\ \Delta G^0 &= -RT \ln \mathrm{K}_0, \\ \ln K_0 &= \frac{\Delta S^0}{R} - \frac{\Delta H^0}{RT}, \end{aligned} \tag{11}$$

where $C_{a,e}$ is the equilibrium quantity of the adsorbent in a solution of unit volume, K_d is the apparent equilibrium constant, K_0 is the equilibrium constant, and the rest is the same as above.

The parameters ΔS^0 and ΔH^0 could be obtained from the slope and intercept of the ln K_0 and $1/T$ plots (Figure 8). The adsorption thermodynamic parameters are listed in Table 5. At different temperatures, ΔG^0 was negative, indicating that

Table 2: Adsorption kinetic parameters.

The pseudo-first-order kinetic			The pseudo-second-order kinetic			Elovich equation		
Q_e (mg/g)	K_1 (/min)	R^2	Q_e (mg/g)	K_2 (mg/g/min)	R^2	A (mg/g)	B (mg/g/min)	R^2
301.098	0.349	0.801	302.661	0.009	0.966	285.173	3.523	0.902

Table 3: The intraparticle diffusion model parameters.

I			II		
K_1 (mg/g/min$^{1/2}$)	C_1 (mg/g)	R^2	K_2 (mg/g/min$^{1/2}$)	C_2 (mg/g)	R^2
1.868	286.707	0.742	0.179	299.938	0.353

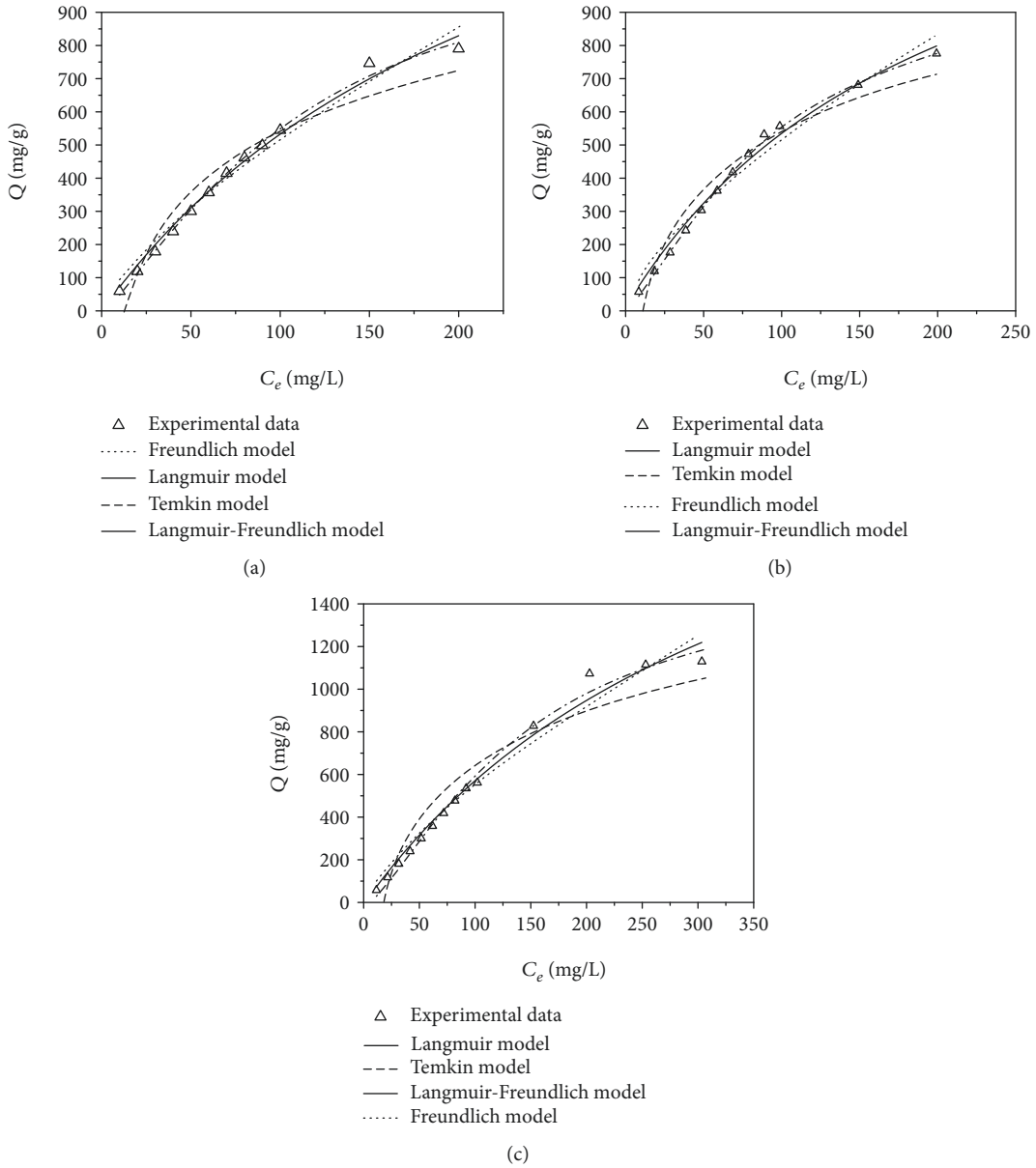

Figure 7: (a) 298K adsorption isotherm of BC/g-C_3N_4 on MB. (b) 308K adsorption isotherm of BC/g-C_3N_4 on MB. (c) 318K adsorption isotherm of BC/g-C_3N_4 on MB.

Table 4: Adsorption isotherm parameters.

(a)

T/K	Langmuir-Freundlich model				Langmuir model		
	Q_m (mg/g)	K_L (L^{α}/mg^{α})	α	R^2	Q_m (mg/g)	K_L (L/mg)	R^2
298	802.581	0.002	1.310	0.996	772.009	0.00398	0.991
308	833.748	0.00175	1.365	0.998	797.265	0.00426	0.989
318	1199.645	0.00089	1.416	0.991	1024.867	0.00470	0.983

(b)

T/K	Freundlich model			Temkin model		
	K_F ($mg^{1-1/n}\ L^{1/n}/g$)	n	R^2	D (mg/g)	E (L/g)	R^2
298	17.207	1.355	0.976	669.153	263.019	0.927
308	17.277	1.327	0.966	740.199	295.710	0.938
318	17.557	1.334	0.967	1025.028	364.215	0.893

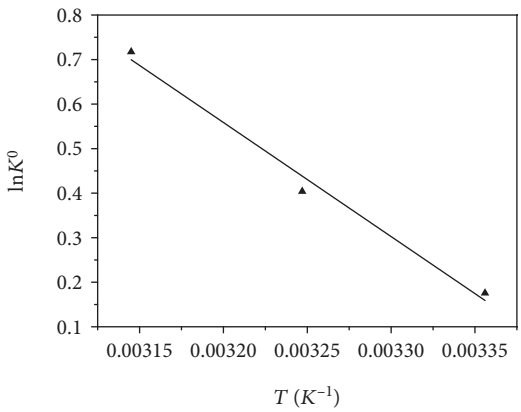

Figure 8: BC/g-C_3N_4 adsorbed MB ln K_0 for $1/T$ fitting.

Table 5: Adsorption thermodynamic parameters.

T/K	ΔG^0 (kJ/mol)	ΔH^0 (kJ/mol)	ΔS^0 (J/mol/K)	R^2
298	-0.435			
308	-1.034	21.300	72.804	0.988
318	-1.897			

the adsorption reaction was spontaneous and beneficial. As the temperature increased, the ΔG^0 value decreased, indicating that the temperature rise was beneficial to the adsorption of MB. The positive value of ΔH^0 indicated that the adsorption of MB in BC/g-C_3N_4 was an endothermic process, and the positive value of ΔS^0 indicates that the disorder of the solid/liquid interface increased during the adsorption of MB in BC/g-C_3N_4 [18].

3.7. Analysis of Adsorption Mechanism. As the BC calcination temperature was increased (400°C, 500°C, and 600°C), the surface had more typical aromatic structures and formed more π-π bonds, and the ionic electrostatic force with MB was weakened [15]. Experimental results (removal rate) are as follows: BC_{300} (95%) > BC_{400} (68%) > BC_{600} (33%) > BC_{500} (29%), indicating that the low temperature cracking had better adsorption properties for MB, so cationic dyes such as MB should be given priority. Biochar with low pyrolysis temperature and high polarity should be considered [15]. Like many other compounds, g-C_3N_4 powder exhibited protonation and deprotonation in an aqueous suspension. The chemical nature of these two processes included interactions between hydrogen ions, hydroxyl ions, and certain groups on the surface of the carbon nitride. Under different pH conditions, the degree of these chemical interactions was different, resulting in different surface charge and zeta potential of g-C_3N_4 samples. C-N heterocyclic and N-H coordination groups on the g-C_3N_4 surface and electrostatic adsorption on the surface played an important role [19].

The pseudo-second-order kinetic fitting results showed that the adsorption of dyes by BC/g-C_3N_4 was mainly through the chemical bond between them. The Langmuir-Freundlich model fitting results showed that the adsorption was not controlled by a single mechanism. The intraparticle diffusion model showed that the adsorption was affected by both internal diffusion and external diffusion. FT-IR showed that the surface of BC/g-C_3N_4 was mainly composed of polar oxygen-containing functional groups (carboxyl, hydroxyl, phenolic hydroxyl, ether, and ester), combined with adsorption curve characteristics and adsorption test of anionic dye methyl orange according to MB experimental scheme. The efficiency was only 13% of that of MB; further, it could be concluded that in BC/g-C_3N_4 there was ion exchange adsorption of cationic dye MB.

4. Conclusion

The adsorption performance of BC/g-C_3N_4 composite was better than that of a single component, especially under alkaline conditions (pH = 11). When the doping ratio was 1 : 3, g-C_3N_4 was more uniformly dispersed on BC and the

number of functional groups increased. To achieve excellent adsorption effect, 0.16 g/L or so was added.

The adsorption process conformed to the pseudo-second-order kinetic model ($R^2 = 0.966$). The reaction was affected by physical and chemical adsorption. The intraparticle diffusion model further demonstrated that the BC/g-C_3N_4 adsorption process included surface adsorption and intraparticle diffusion.

The Langmuir-Freundlich model can describe the adsorption process well under different temperature conditions ($R^2 > 0.99$). It is calculated by thermodynamic parameters that the reaction is spontaneous ($A < 0$). The reaction was endothermic reaction and the degree of disorder increased as the temperature increases ($B > 0$, $C > 0$).

Under different temperature conditions, the Langmuir-Freundlich model could describe the adsorption process well ($R^2 > 0.99$). The thermodynamic parameters were calculated and the reaction proceeded spontaneously ($\Delta G^0 < 0$). The reaction was endothermic reaction and the degree of disorder increased as the temperature increased ($\Delta H^0 > 0$, $\Delta S^0 > 0$).

Data Availability

The data used to support the findings of this study are included within the article.

Conflicts of Interest

The authors declare that they have no conflicts of interest.

Acknowledgments

This work was supported by the Natural Science Foundation of Jilin Province Department of Education (no. JJKH20170241KJ and no. JJKH20190857KJ).

References

[1] E. B. Belal, "Bioethanol production from rice straw residues," *Brazilian Journal of Microbiology*, vol. 44, no. 1, pp. 225–234, 2013.

[2] S. Elumalai, B. Agarwal, T. M. Runge, and R. S. Sangwan, "Integrated two-stage chemically processing of rice straw cellulose to butyl levulinate," *Carbohydrate Polymers*, vol. 150, pp. 286–298, 2016.

[3] S. Wi, I. Choi, K. Kim, H. Kim, and H.-J. Bae, "Bioethanol production from rice straw by popping pretreatment," *Biotechnology for Biofuels*, vol. 6, no. 1, pp. 166-167, 2013.

[4] Y. Qiu, Z. Zheng, Z. Zhou, and G. D. Sheng, "Effectiveness and mechanisms of dye adsorption on a straw-based biochar," *Bioresource Technology*, vol. 100, no. 21, pp. 5348–5351, 2009.

[5] D. De, S. Santosha, V. Aniya, A. Sreeramoju, and S. B, "Assessing the applicability of an agro-industrial waste to engineered bio-char as a dynamic adsorbent for fluoride sorption," *Journal of Environmental Chemical Engineering*, vol. 6, no. 2, pp. 2998–3009, 2018.

[6] M. A. Zazycki, M. Godinho, D. Perondi, E. L. Foletto, G. C. Collazzo, and G. L. Dotto, *Journal of Cleaner Production*, vol. 171, pp. 57–65, 2018.

[7] J. Chen, W. Xiaohui, W. Hao, and J. Qi, "Study on decolorization of dyeing wastewater by electrochemical treatment," *IOP Conference Series: Earth and Environmental Science*, vol. 113, article 12207, 2018.

[8] S. el-Kacemi, H. Zazou, N. Oturan et al., "Nanostructured ZnO-TiO_2 thin film oxide as anode material in electrooxidation of organic pollutants. Application to the removal of dye Amido Black 10B from water," *Environmental Science and Pollution Research*, vol. 24, no. 2, pp. 1442–1449, 2017.

[9] M. Bahia, F. Passos, O. F. H. Adarme, S. F. Aquino, and S. Q. Silva, "Anaerobic-aerobic combined system for the biological treatment of azo dye solution using residual yeast," *Water Environment Research*, vol. 90, no. 8, pp. 729–737, 2018.

[10] I. Ali and V. K. Gupta, "Advances in water treatment by adsorption technology," *Nature Protocols*, vol. 1, no. 6, pp. 2661–2667, 2006.

[11] L. Pi, R. Jiang, W. Zhou et al., "g-C3N4 modified biochar as an adsorptive and photocatalytic material for decontamination of aqueous organic pollutants," *Applied Surface Science*, vol. 358, pp. 231–239, 2015.

[12] S. Fan, Y. Wang, Z. Wang, J. Tang, J. Tang, and X. Li, "Removal of methylene blue from aqueous solution by sewage sludge-derived biochar: adsorption kinetics, equilibrium, thermodynamics and mechanism," *Journal of Environmental Chemical Engineering*, vol. 5, no. 1, pp. 601–611, 2017.

[13] Y. Sun, Z. Y. Wu, X. Wang et al., "Macroscopic and microscopic investigation of U(VI) and Eu(III) adsorption on carbonaceous nanofibers," *Environmental Science & Technology*, vol. 50, no. 8, pp. 4459–4467, 2016.

[14] E. Bulut, M. Özacar, and İ. A. Şengil, "Adsorption of malachite green onto bentonite: equilibrium and kinetic studies and process design," *Microporous and Mesoporous Materials*, vol. 115, no. 3, pp. 234–246, 2008.

[15] X. Q. Ji, L. Lü, F. Chen, and C. P. Yang, "Sorption properties and mechanisms of organic dyes by straw biochar," *Acta Scientiae Circumstantiae*, vol. 36, no. 5, pp. 1648–1654, 2016.

[16] P. Patil, Y. Marathe, and V. Shrivastava, "Evaluation of the adsorption kinetics and equilibrium for the potential removal of congo red dye from aqueous medium by using a biosorbent," *British Journal of Applied Science & Technology*, vol. 6, no. 6, pp. 557–573, 2015.

[17] M. H. Khani, "Uranium biosorption by *Padina* sp. algae biomass: kinetics and thermodynamics," *Environmental Science and Pollution Research*, vol. 18, no. 9, pp. 1593–1605, 2011.

[18] G. Zhao, J. Li, X. Ren, C. Chen, and X. Wang, "Few-layered graphene oxide nanosheets as superior sorbents for heavy metal ion pollution management," *Environmental Science & Technology*, vol. 45, no. 24, pp. 10454–10462, 2011.

[19] B. Zhu, P. Xia, W. Ho, and J. Yu, "Isoelectric point and adsorption activity of porous g-C3N4," *Applied Surface Science*, vol. 344, pp. 188–195, 2015.